Title
Modeling of CO2 sequestration in coal seams: Role of CO2-induced coal softening on injectivity, storage efficiency and caprock deformation

Journal
Greenhouse Gases Science and Technology, 7(3)

ISSN
2152-3878

Authors
Ma, Tianran
Rutqvist, Jonny
Liu, Weiqun
et al.

Publication Date
2017-06-01

DOI
10.1002/ghg.1664

Peer reviewed

Modeling of CO_2 sequestration in coal seams: role of CO_2-induced elastic properties variation of coal on injectivity, storage efficiency and caprock deformation

Tianran Ma [a, c], Jonny Rutqvist [b], Weiqun Liu [a]

[a] State Key Laboratory for Geomechanics and Deep Underground Engineering, China University of Mining and Technology, Xuzhou, Jiangsu, China

[b] Lawrence Berkeley National Laboratory, Earth Sciences Division, Berkeley, CA, USA

[c] Department of Civil and Environmental Engineering, University of Alberta, Edmonton, Canada

This is the version submitted for publication in

Greenhouse Gas Sciences & Technology

The final version is published as:

Ma T., Rutqvist, J., Liu, W., Zhu L., Kim, K. Modeling of CO2 sequestration in coal seams: role of CO2-induced coal softening on injectivity, storage efficiency and caprock deformation. Greenhouse Gas Sciences & Technology., 7, 562-578 (2017). DOI: 10.1002/ghg.

Abstract

An effective and safe operation for sequestration of CO_2 in coal seams requires a clear understanding of injection-induced coupled hydromechanical processes such as the evolution of pore pressure and permeability as well as induced caprock deformation. In this study, CO2 injection into coal seams was studied using a coupled flow-deformation model with a new stress-dependent porosity and permeability model that considers CO2-induced elastic property variation. . Based on triaxial compression tests of coal samples extracted from the site of the first enhanced coalbed methane field tests in China, a substantial (one-order-of-magnitude) softening of Young's modulus and increase of Poisson's ratio with adsorbed CO_2 content was observed. Such coal softening was considered in the numerical simulation through an exponential relation between elastic properties (Young's modulus and Poisson's ratio) and CO_2 pressure, considering that adsorbed CO_2 content is proportional to the CO_2 pressure. The results of the numerical simulation show that the combination of softening of the coal and enhancement of Poisson's ratio strongly affects the CO_2 sequestration performance, by decreases of injectivity and stored volume (cumulative injection) during first ten days of injection, and thereafter a softening mediated rebound in permeability tends to increase injectivity and storage with time. A sensitivity study showed that hydromechanical characteristics including large softening coefficient, high initial permeability and porosity, large initial Young's modulus and Poisson ratio and high injection pressure all contribute synergistically to increase CO_2 injectivity and adsorption in coal seams, but also result in larger caprock deformations. Overall, the study demonstrates the importance of considering the CO_2-induced variations in elastic coal properties when analyzing the performance and environmental impact of a CO_2-sequestration operation in uminable coal seams.

***Keywords*: CO_2 sequestration; Coal seams; Elastic modulus softening; Poisson's ratio rising; Caprock deformations;**

1. Introduction

CO_2 emitted during industrial burning of fossil fuels intensify the greenhouse effect that poses a serious long-term threat to the human living environment. Carbon capture and storage (CCS) is recognized as a promising approach to reduce CO_2 emission to the atmosphere and avoid further pollution of the natural environment (Rubin, 2005). CCS refers to a type of technology that captures CO_2 from the combustion of fossil fuels during industrial processes and store (or sequester) it deep underground. In geologic formations, CO_2 can be stored in oil and gas reservoirs, saline aquifers and coal seams (Bachu, 2008; Rutqvist and Tsang, 2002; Van Bergen et al., 2004; Haszeldine, 2009; Ferronato et al., 2010; Gou et al., 2014). Among the geological sequestration options, storage of CO_2 in deep and unminable coal seams havs gained industrial attention because of its value added associated with Enhanced CoalBed Methane (ECBM) production (White et al., 2005).

The storage of CO_2 in coal seams is a promising technology and a rational choice. In particular, the parts of coal seams that are not suitable for coal extraction offer a tremendous potential for sequestering CO_2 (Gale, 2004). The trapping mechanism for the storage of CO_2 in coal seams is different from those in saline aquifers and hydrocarbon reservoirs. Coal is a naturally fractured dual-porosity media consisting of cleat and matrix systems (Warren and Root, 1963; Gray, 1987). Fractures and pores in cleat systems provide pathways for CO_2 seepage, while the micropores and grains in the matrix system act as the principal storage space where large quantities of CO_2 can be adsorbed. The CO_2 should stay adsorbed in the unminable coal as long as the reservoir pressure is above the desorption pressure (Shukla et al., 2010). Injection and storage of CO_2 in coal seams can also efficiently improve the production rate of coalbed methane (CO_2-ECBM) as have been observed in the field (e.g., Zakkour and Haines, 2007). Another important factor to consider related to storage of CO_2 in coal seams is that the adsorbed CO_2 can act as a type of plasticizer, which can alter the structure of a coal seam, which seems to improve the porosity and thereby increase the CO_2 injectivity and storage capacity (Goodman et al., 2006; Shukla et al., 2010).

The plasticizing effect of adsorbed CO_2 can be expected to weaken the coal and thus result in a reversible decrease of elastic modulus and strength (Ates and Barron, 1988; Viete and Ranjith, 2006; Masoudian et al., 2014). For example, uniaxial compression testing by Viete and Ranjth (2006) showed that the elastic modulus could decrease by approximately 26%. Based on results from recent triaxial compression experiments, Masoudian et al. (2014) proposed a Langmuir-type relationship between the reduction in elastic modulus of bituminous black coal and adsorbed CO_2. However, in the study of Viete and Ranjith (2006), no obvious reduction in elastic modulus was found in experiments at high confining stress. This lack of weakening at high confining stress could be explained by decreased CO_2 adsorption at high confining stress (Hol et al., 2011).

With CO_2 injection into coal seams, the free and adsorbed CO_2 could disturb the balance in the reservoir and induce changes in pore pressure and stress and cause heterogeneous swelling (Reucroft and Patel, 1986), which in turn, could significantly affect the permeability distribution within the coal seam. During CO_2 injection into a coal seam, the permeability is mainly controlled by the pore pressure and adsorption-induced swelling and their impact on the cleat system. An increase in pore pressure leads to a decrease in effective stress and thus enhances coal permeability. In contrast, the swelling of the coal matrix induced by the adsorption of CO_2 decreases the permeability (Siriwardane et al., 2009; Liu and Rutqvist, 2010).

A number of porosity and permeability models have been proposed to represent the effects of pore pressure and CO_2-adsorption-induced swelling on the evolution of permeability/porosity. The S&H model (Seidle and Huitt, 1995) assumes that permeability changes are only caused by coal matrix swelling. The P&M model (Palmer and Mansoori, 1998) includes a theoretical equation for porosity as a function of pore pressure, incorporating the effects of elastic properties and sorption-induced strain for low-porosity (less than 1) coal seams under uniaxial stress conditions. Exponential forms are frequently used to formulate changes in porosity and permeability as a function of fluid pressure. Two well-known exponential permeability models, the S&D (Shi and Durucan, 2004) model and C&B (Cui and Bustin, 2005) model, were developed for conditions of uniaxial strain and assuming that the horizontal stress and mean normal stress affect the permeability and porosity, respectively. In both of these models, the pore modulus is simplified to be constant, though pore modulus in coal actually varies with porosity and stress (Detournay and Cheng, 1993). Another exponential permeability model by Liu and Rutqvist (2010) considers fracture–matrix interaction during coal-deformation processes based on the concept of internal swelling stress, which can explain experimental data showing permeability decrease with CO_2 adsorption under constant confining stress.

In this paper, a coupled flow-deformation model that employs a new stress-dependent porosity and permeability model and considers CO_2-induced coal softening and Poisson's ratio variation are applied to study CO_2 injection into coal seams. Though experimental evidence of substantial softening of coal and variation of Poisson's ratio with CO_2 content, such elatic property variations have generally not been considered in previous analyses of CO_2 sequestration operations in unminable coal. The objective of this study is to investigate the effects of such CO_2-induced coal softening and Poisson's ratio variation on the performance of CO_2 sequestration into coal seams. In this paper, we first provide the theoretical background and derive governing equations related to coupled fluid flow and mechanical deformations, including a new model for permeability evolution that considers coal swelling and CO_2-induced coal softening and Poisson's ratio variation. The governing equations are implemented and solved with the multi-physics software COMSOL, which is then applied for the study of coupled fluid flow and deformations during CO_2 injection into coal seams. The simulation results are presented to demonstrate the effects of elastic modulus softening and Poisson's ratio variation on permeability, injectivity, storage efficiency and deformations. In addition, the implications of the elastic property variations, hydraulic properties (porosity and permeability) and elastic properties (Young's modulus and Poisson ratio) of coal seams and injection pressure are studied in a sensitivity analysis. Overall, the study demonstrates the importance of considering the CO_2-induce softening when analyzing the performance and environmental impact of CO_2-sequestration in uminable coal seams.

2. Governing and Constitutive Equations

2.1. Coal seam deformation

On the basis of the constitutive relation of poroelasticity, stress equilibrium, effective stress law, and considering CO_2-adsorption-induced volumetric strain (Cui and Bustin, 2005), the governing equation for deforming coal seams can be expressed as follows (Rutqvist et al., 2001):

$$\sigma = \sigma' - \alpha I p = D : (\varepsilon - \varepsilon_s \delta) - \alpha I p \quad (1) \qquad (1)$$

where α is Biot's coefficient, σ and σ' are total and effective stress tensors, p is pore pressure, D is the tangential stiffness matrix and ε_s is the sorption-induced volumetric strain calculated by the Langmuir-type equation as:

$\varepsilon_s = \varepsilon_L \dfrac{p}{p + p_L} (2)$ where ε_L and p_L represent the Langmuir volumetric strain and Langmuir pressure constants, respectively.

2.2. Gas flow

The CO_2 mass balance equation for coalbed methane includes adsorption, diffusion and seepage and is defined as:

$$\frac{\partial m}{\partial t} + \nabla \cdot (\rho_g \vec{v}_g) = Q_s (4)$$

where ρ_g is the gas density, $\vec{v}_g$ is the Darcy velocity vector, t is time, Q_s is the gas source, and m is the gas content, which includes the free and adsorbed CO_2 and is defined as (Zhang et al., 2008):

$$m = \rho_g \phi + \rho_{ga} \rho_c \frac{V_L p}{p + p_L} (5)$$

where ϕ is the porosity of the cleat system, V_L is the Langmuir volume constant, ρ_c is coal density and ρ_{ga} is CO_2 density under standard conditions.

According to the ideal gas law, gas density is given by:

$$\rho_{ga} = \frac{p}{p_a} \rho_g (6)$$

where p_a is the standard atmospheric pressure. In addition, gas-flow through the cleats according to Darcy's law without the gravity effect is expressed as:

$$\vec{v}_g = \frac{-k}{\mu} \nabla p \quad (7)$$

where k is the permeability of the coal cleat system, and μ is the gas viscosity.

Substituting Eqs. (5), (6) and (7) into Eq. (4) gives the following governing equation for gas flow in the cleat system:

$$\left[\phi + \frac{\rho_c p_a V_L p_L}{(p+p_L)^2}\right]\frac{\partial p}{\partial t} + p\frac{\partial \phi}{\partial t} + \nabla \cdot \left(\frac{-k}{\mu} p \nabla p\right) = Q_s \quad (8)$$

From Eq. (8), the partial derivative of ϕ with respect to time is expressed as

$$\frac{\partial \phi}{\partial t} = S\left(\frac{-1}{K}\frac{\partial \sigma'}{\partial t} + \frac{\alpha - 1}{K}\frac{\partial p}{\partial t}\right) \quad (14)$$

where $S = (\phi_0 - \alpha)\exp\left\{\frac{-1}{K}\left[(\sigma' - \sigma'_0) + (1-\alpha)(p - p_0)\right]\right\}$

Substituting Eq. (14) into Eq. (8), the governing equation yields

$$\left\{\phi + \frac{\rho_c p_a V_L p_L}{(p+p_L)^2} + \frac{pS(\alpha - 1)}{K}\right\}\frac{\partial p}{\partial t} + \nabla \cdot \left(\frac{-k}{\mu} p \nabla p\right) = Q_s + \frac{pS}{K}\frac{\partial \sigma'}{\partial t} \quad (15)$$

Eqs. (15) and (1) are the governing equations for gas flow and mechanics, respectively, that will be solved considering various couplings, including those related to elastic property variations with CO_2 content and permeability variation with effective stress and swelling. These processes will be described in detail in the next two subsections.

2.5 Elastic property variation with CO_2 content

In this paper, the results of triaxial compression tests on coal specimens are used to derive a relationships for howelastic modulus and Poisson’s ratio changes withCO_2 with adsorbed CO_2 content. Because adorbed CO_2 is a function of CO_2 pressure, we directly relate elastic properties to CO_2 overpressure, which is the gas pressure applied by injection minus the initial pressure in the coal specimens. The initial pressure within the coal specimens was equal to atmospheric pressure, which correspond to such a small CO_2 content that it has no significant influence on the elastic properties. The dimension, test conditions and elastic modulus of the coal specimens are listed in Table 1. Specimens with a diameter of about 50 mm and a height of about 102 mm were prepared from drill cores obtained from a mine in the Qinshui Basin, which is the site the first CO_2 enhanced coalbed methane (CO_2-ECBM) recovery single-well micro-pilot tests in China (Wong et al., 2010; Li and Fang, 2014). The CO_2-saturated specimens were prepared by permeating CO_2 at different pressure for 24 hours to ensure the desired saturation level. The triaxial tests were carried out with a loading rate of 1 MPa/min until the confining pressure reached 5.0 MPa and then the specimens were loaded axially to failure under a displacement rate of 0.005 mm/s.

Table 1

Dimension, test conditions, elastic modulus and Poisson's ratio of coal specimens

NO.	diameter (mm)	Height (mm)	Confining Pressure (MPa)	Overpressure (MPa)	Elastic Modulus (GPa)	Poisson's ratio
1	49.62	102.56	5.0	4.52	1.188	0.372
2	49.74	101.78	5.0	3.56	1.8	0.365
3	49.72	102.66	5.0	2.58	2.469	0.315
4	49.62	101.20	5.0	0	4.018	0.286

The Young's modulus and Poisson's ratio versus overpressure for the experimental results are plotted in Fig. 1 (red points). It can be clearly observed that the elastic modulus decreases and Poisson's ratio increases with the increase in overpressure. The experimental data of Young's modulus is fitted to an exponential relation written as

$$E = E_{max} \exp(-a \times \Delta p) \quad (9)$$

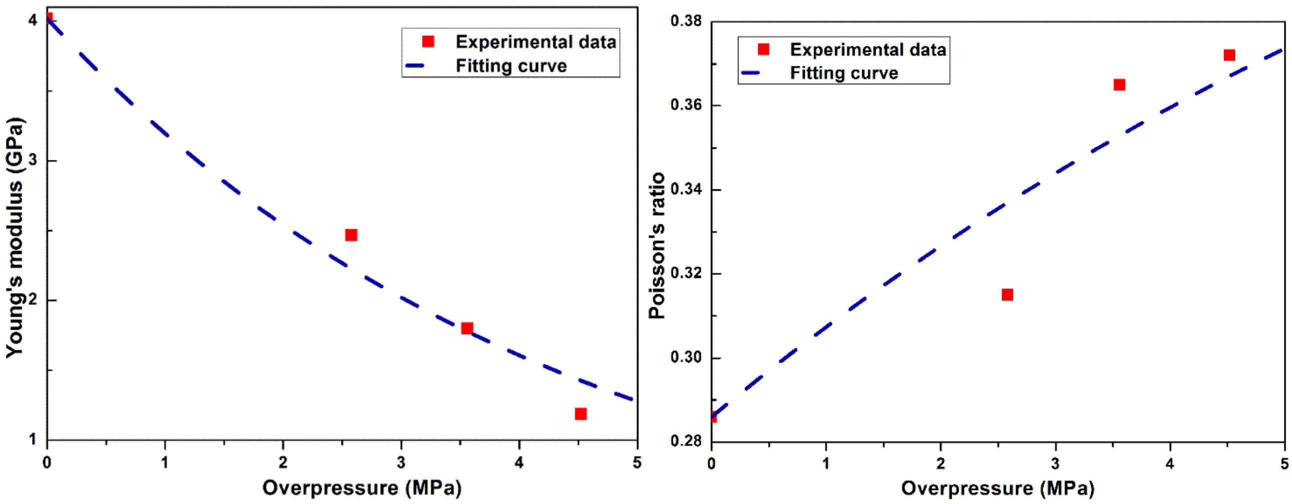

Fig. 1. Exponential relationship between Young's modulus and Poisson's ratio, and overpressure

The Poisson's ratio is related to overpressure according to

υ
¿
m
$¿0-\upsilon_{¿}$
¿
$\upsilon = \upsilon_m + ¿$

where Δp is the over pressure. E_{max} is the maximum/initial elastic modulus with no significant amount of CO_2 adsorbed in the coal, i.e. at low or atmospheric pressure. υ_0 is Poisson's ratio at zero overpressure and υ_m is the limiting value of 0.5. The exponents *a* and *b* in Eqs. (9) and (10), are coefficients determining the rate of variability with increasing CO_2 overpressure. A larger a and b would result in more decrease of E and increase of υ with overpressure. In this case, a and b are estimated to 0.2291 and 0.1054, respectively, by matching the exponential model to experimental data (Fig.1) using a least squares method with reasonable coefficients of determination ($R^2=0.9737$ and $R^2=0.8716$).

2.3 Evolution of porosity and permeability

An increase of pore pressure during CO_2 injection will expand the pore volume resulting in increased porosity and permeability. While considering gas migration through a coal seam with desorption or adsorption, the changes in gas pressure (and gas concentration) induces coal swelling or shrinkage that in turn changes coal porosity and permeability. In this study, a new model relating porosity to mean effective stress is built based on the C&B model (**Appendix A**):

$$\phi=\alpha+(\phi_0-\alpha)\exp\left\{\frac{-1}{K}\left[\left(\sigma'-\sigma'_0\right)+(1-\alpha)(p-p_0)\right]\right\} \quad (11)$$

Without consideration of the Klinkenberg effect, a cubic law is used to describe the relationship between the permeability and porosity of the porous media, which is shown as follows

$$\frac{k}{k_0}=\left(\frac{\phi}{\phi_0}\right)^3=\left\{\frac{\alpha}{\phi_0}+\frac{(\phi_0-\alpha)}{\phi_0}\exp\left\{\frac{-1}{K}\left[\left(\sigma'-\sigma'_0\right)+(1-\alpha)(p-p_0)\right]\right\}\right\}^3 \quad (12)$$

where ϕ_0 and k_0 represent the initial porosity at pressure p_0 and the initial effective stress.

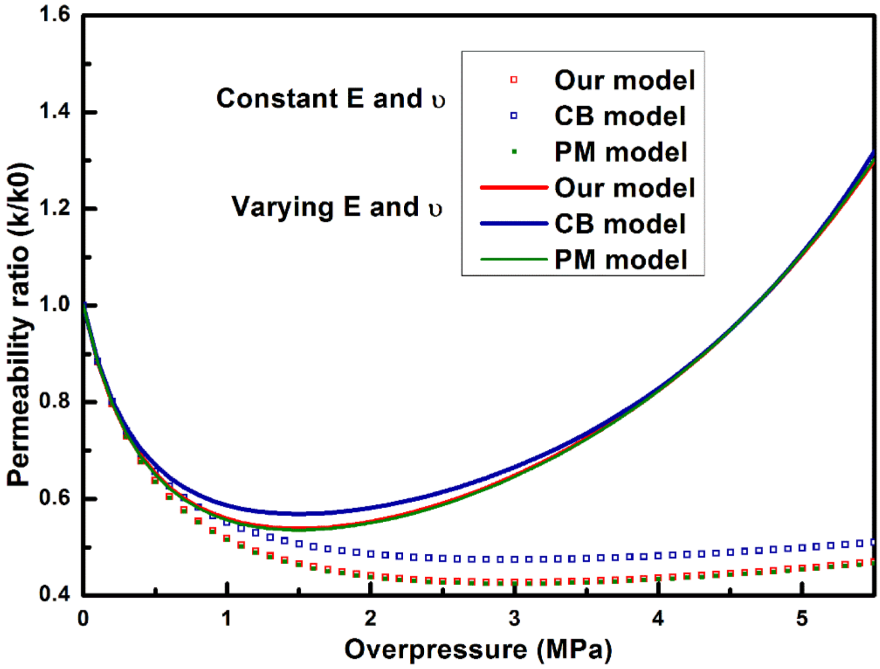

Fig. 2. Influence of elastic modulus on the proposed permeability model, C&B and P&M models. Poisson's ratio of 0.35, an initial reference permeability of 1 × 10^{-14} m^2, an initial reference porosity of 0.8%, an injection pressure of 6 MPa and an initial coal-seam pressure of 0.5 MPa are assumed for all three models.

Assuming that the coal-seams are under conditions of uniaxial strain, constant coal-seam loading and $\alpha=1$, our model, C&B model and P&M model are expressed as in Eqs. (A.18), (A.19) and (A.20), respectively The permeability ratio versus pressure for the three models are plotted in Fig. 2. The red line is the model proposed in this paper, the green and the blue lines represent the C&B and P&M models, respectively. The solid lines are the evolution of the permeability ratio with a varying elastic modulus E and Poisson's ratio υ described in Eqs. (9) and (10), wheareas the square symbols represent permeability evolution when assuming constant E and υ.. The Langmuir-type relationship between pore pressure p and adsorption induced strain ε_s increases strongly at early time, while the change of ε_s is more flat at a higher injection pressure at later time. Thus, a clear decline in permeability is observed in all three models for both cases from its initial value with increasing pressure as a result of strong swelling of coal matrix. Then, it has no obviously rebound with a constant E and υ ($E=4.018\,GPa$, $\upsilon=0.286\,GPa$), but enhances up to a 1.3 times (solid lines) with the combination of a varying E and υ , as a result of reduced adsorption effect and dominance of pore pressure effect. The pressure where permeability starts to rebound is called as the rebound pressure (Shi and Durucan, 2004), which is given as (Cui and Bustin, 2005)

$$p_{rb}=\sqrt{\frac{E\,\varepsilon_s V_L p_L}{3v}}-p_L \quad (13)$$

From the equation, an increase of Poisson's ratio and a decrease of Young's modulus both reduce the rebound pressure that advances the permeability rebound. In two cases, permeability in C&B model predicts an obvious larger value than P&M and our model without consideration of the changes in the pore modulus. The value of permeability in our model is similar to the P&M model. This is because the P&M model can be deduced by Taylor expansion for the exponential function in our model.

3. Numerical Implementation

The governing Equations and constitutive relations described above are implemented within COMSOL Multiphysics, which is an efficient visual platform for simulating and analyzing coupled phenomena with finite elements method (http://www.comsol.com/). Two pre-arranged modules named Geomechanics and Fluid Flow are selected to solve the partial differential equations (PDEs). The schematic of solving coupled CO_2 flow and coal seam deformation in COMSOL, including governing equations and coupling relationsare illustrated in Fig. 3.

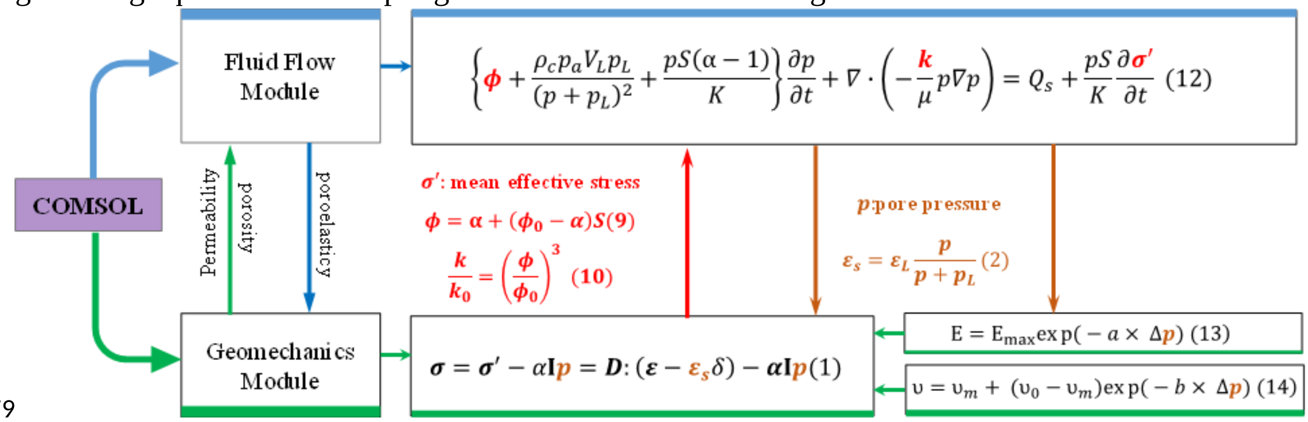

Fig. 3. Schematic of modeling coupled CO_2 flow and coal seam deformation in COMSOL

First, the model geometry is built in the COMSOL graphic window. Thereafter, various material properties are assigned, including density and viscosity of CO_2 and permeability, porosity, density, elastic modulus and passion's ratio of the coal seam and surrounding rock The boundary and initial conditions are also set in the two modules. For CO_2 flow, pressure and no flow boundary conditions are defined:

$$p = p_0 \text{ on } \partial\Omega \; ; \quad -n\cdot\rho u = 0 \text{ on } \partial\Omega \quad (16)$$

Here p_0 is the specified CO_2 pressure on the boundary $\partial\Omega$, n is the vector normal to the boundary, ρ is gas density and u is the velocity vector. The initial condition for flow is:

$$p(0) = p \text{ in } \Omega \quad (17)$$

For geomechanics module, displacement and stress conditions are specified on the boundary as

$$u = u_0 \text{ on } \partial\Omega \; ; \quad s\cdot n = F_A \text{ on } \partial\Omega \quad (18)$$

where u_0 and F_A are the prescribed displacement and stress on the boundary $\partial\Omega$ and S is stress symbol in COMSOL. The initial conditions for displacement and *in-situ* stress in the domain are described as

$$u(0)=0\in ¿ \quad \Omega \; ; \; s(0)=s\in ¿ \quad \Omega \qquad (19)$$

Finally, in the simulation conducted in this paper a default MUMPS solver was employed to solve all the equations in a fully coupled (monolithic) mode. Note that in this modeling we selected a relatively small absolute and relative tolerance (compared to default settings) for a stringent and accurate solution. It makes the model run slightly slower, but it is an efficiency method to stabilize convergence and improve the precision of the calculation.

4. Geometry and material properties

Fig. 4 illustrates a conceptual model of CO_2-injection from a horizontal well (on the left) and the two-dimensional computational model geometry for the analysis of CO_2 injection into a coal seam. The choice of a horizontal well configuration is a pragmatic one, simplifying the model geometry to a two-dimensional plane strain model. However, in the field a horizontal well configuration could be beneficial by accessing a larger reservoir area and being able to take advantage of known anisotropic permeability and thereby help alleviate permeability reduction and injectivity loss in a CO2-ECBM and/or CO2 storage project (Durucan and Shi, 2009). The injection formation (coal seam) has a thickness of 6.45 m and the model is extends 300 m horizontally, which ensures that the overpressure does not reach the right boundary over the time scale of the simulation. The coal seam is bounded by a 50-m thick basement and a 43.55-m thick caprock, and half of a horizontal well is modeled at the symmetry plane of the left lateral boundary. The permeability of the caprock and basement was assumed to be small enough so that the injected CO_2 is completely confined within the coal seam. In other words, the gas only flows within the coal seam and no gas leaks into the caprock and basement.

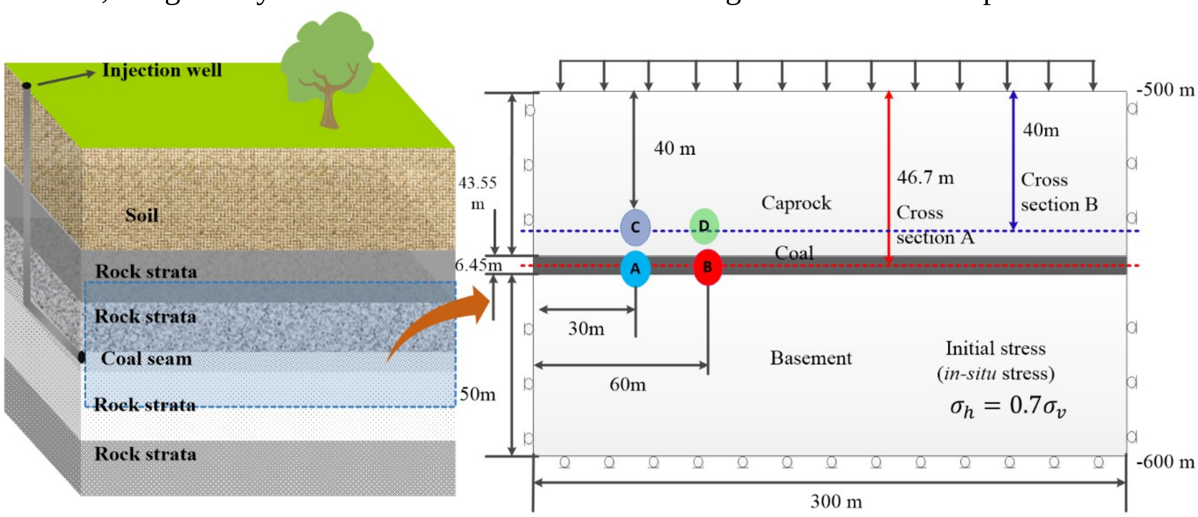

Fig. 4. 3D conceptual model and geometric configuration and 2D computational model domain with initial and boundary conditions

In the simulations, CO_2 was injected from the simulated wellbore located at the mid elevation of left boundary of the coal seam. The injection pressure was linearly increased to 6 MPa in the first two days and then kept constant. The initial pore pressure of CO_2 in coal-seam was assumed to be 0.5 MPa, which assumes that CO_2 injection commences into a coal seam previously pressure depleted by primary production and is gas saturated (Kumar et al., 2014). In this model, the top of the caprock is located at the depth of 500 and has a vertical boundary loading of 11.3 MPa corresponding to the weight of the overburden for an average overburden rock density of 2300 kg/m^3. An extensional stress regime ($\sigma_h = 0.7\,\sigma_v$) was assumed. Displacement constraints were assigned normal to the left, right and bottom boundaries. First, a stationary study was carried out to ensure equilibrium and correct *in-situ* and effective stress vertical gradients at the start of the coupled simulation of the CO_2 injection. All of the simulation cases were meshed with the dense triangular element discretization shown in Fig. 5 to minimize interpolation errors. The coal and CO_2 properties listed in Table 2 are taken from the results of history matching of a micro-pilot test at Qinshui (Wong et al., 2007). In addition, The Biot's coefficient α for the coal seam is assumed to be 0.57 calculated by Eq. (A3) with coal grains Young's modulus of 8.14 GPa (Zhang et al., 2008), fluid viscosity is 1.6×10^{-5}. The caprock and basement are assumed impermeable having Young's modulus of 25 and 30 GPa and Poisson's ratio of 0.339 and 0.25. That is the rock units above and below the coal seam is significantly stiffer than the coal seam.

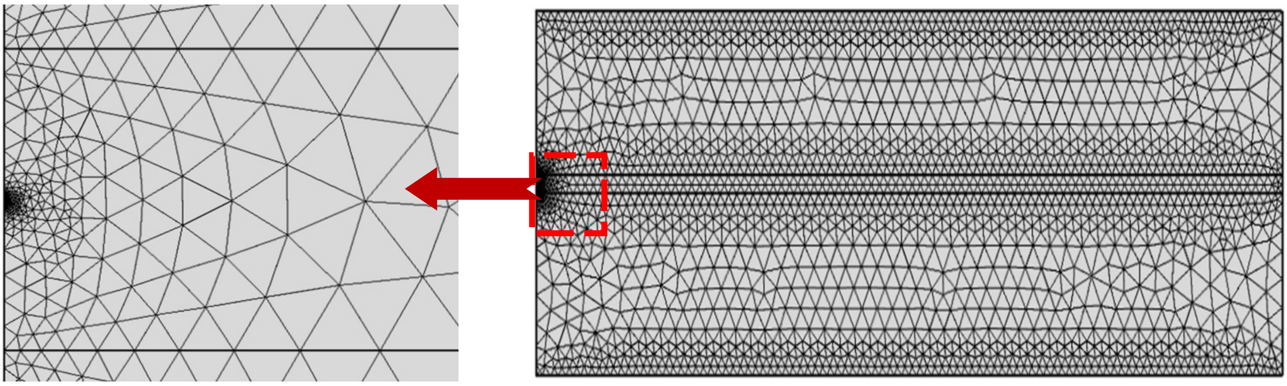

Fig. 5. Finite element mesh in COMSOL (on the right). The figure on the left shows a close-up view of mesh near the injection boundary.

Table 2

Parameters for the coal seam from history matching of a micro-pilot test at Qinshiu (Wong et a., 2007)

Total coal thickness (m)	6.45
[illegible]	0.8
[illegible]	[illegible]
[illegible]	[illegible]
[illegible]	[illegible]
[illegible]	[illegible]
[illegible]	[illegible]
[illegible]	[illegible]
[illegible]	[illegible]

5. Simulation results and discussion

To explore the effects of coal softening on CO_2 sequestration into coal seams, the following two numerical simulation cases were defined:

Case A: The elastic modulus of coal softens during CO_2 injection as a result of overpressure (and CO_2 concentration), as described by Eq. (13).

Case B: Elastic modulus is assumed to be constant and equal to the initial elastic modulus of 3.5 GPa.

We consider Case A, including modulus softening as the base case and by comparing the simulation results for Case A and Case B we can study the effect of coal softening on the CO2 injection performance.

5.1 Simulation results

Fig. 6 shows the distributions of overpressure along cross-section A in the coal seam after 1, 20 and 60 days of injection for four the different cases. The overpressure range of the coal seam with increasing pore pressure keeps expanding away from the gas injection well. After 60 days of injection, gas pressure has already propagated approximately 180 m for case A and C (purple and blue solid lines) and 220 m for case B and D (green and red solid lines) away from the well. The result shows that in the injection process the speed at which the gas pressure front propagates into the coal seam is different for the four cases. After 1 day of injection, there is no clear difference (dotted lines in Fig. 6). Thereafter, the pressure in case B with a constant modulus E and variable Poisson's ratio υ (green dashed line in Fig. 6) propagates farthest (about 110m). At the later stage (after 60 days injection), the pressure in cases with varying υ (green and red solid lines) propagates faster and farther into the coal seam than cases with constant υ (purple and blue solid lines). The pressure in the case with a softening elastic modulus E (blue and red solid lines) is larger near the wellbore, while smaller away from the wellbore.

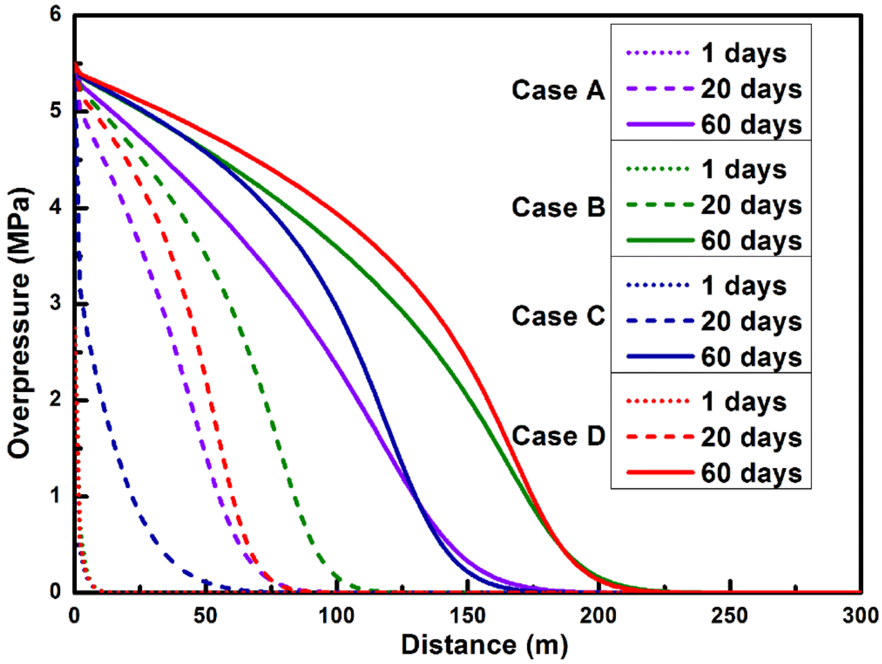

Fig. 6. Distributions of overpressure for four the different cases after 1, 20 and 60 days of injection CO_2

Fig. 7 shows Young's modulus and the Poisson's ratio along cross-section A in the coal seam after 1, 20 and 60 days of injection for the four different cases. As the overpressure in the coal seam increases, Young's modulus decreases and Poisson's ratio increases according to the experimentally fitted exponential relationship in Eqs. (9) and (10). In Fig. 7, the reduction of the modulus E and enhancement of Poisson's ratio υ of can be observed as far as the overpressure propagates, i.e. 180 and 220 m for E (blue and red solid lines in Fig. 7a) and 220 m for υ (green and red solid lines in Fig. 7b) from the injection well. The minimum E and υ are approximately 1.00 GPa and 0.415 close to the wellbore.

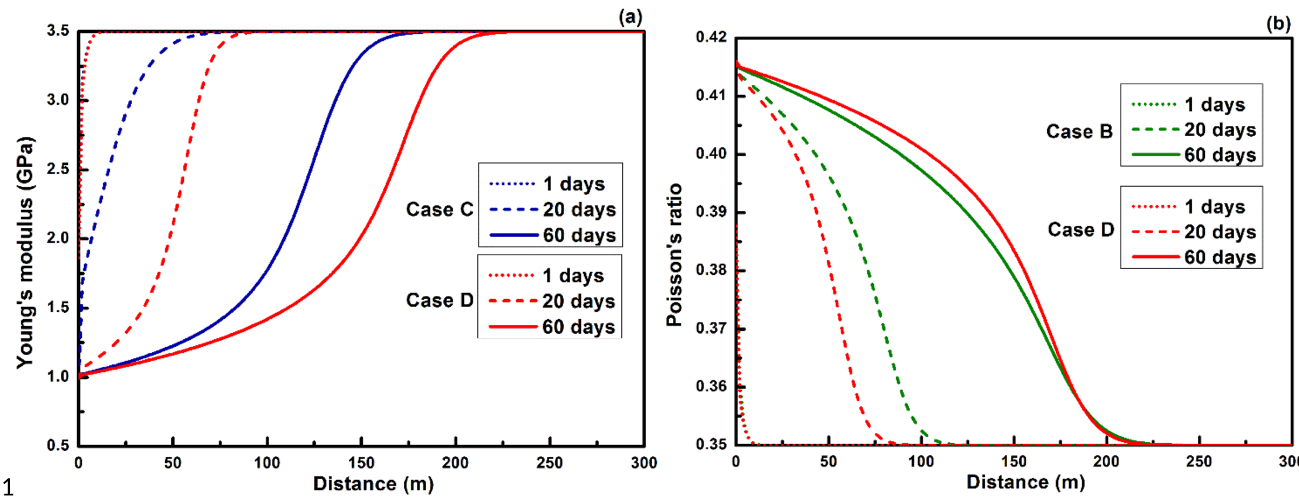

Fig. 7. Profiles of Young's modulus (a) and Poisson's ratio (b) along cross section A at the mid-elevation of the coal seam after 1, 20 and 60 days.

The time-evolution of permeability ratio (k/k_0 , where k_0 is the initial permeability) and pore pressure at two points (A, B) along the horizontal direction is shown in Fig. 8 for the four different cases. At early stages, before the overpressure reached points A and B the permeability in all the cases (Fig. 8a) increase. This change in permeability ahead of the pressure can be explained by the fact that strain and displacement can propagate ahead of the pressure front in a porous elastic media. The peak permeability is largest in Case B with a varying Poisson's ratio υ (green lines in Fig. 8a), whereas the peak permeability increase is much smaller for Case C and D (blue and red lines in Fig. 8a) with a softening elastic modulus E . This demonstrates that an increasing υ promotes the enhancement of permeability and a soften modulus E has an opposite effect. After overpressure reaches points A and B, permeability decreases with increasing overpressure as a results of dominant effect of swelling. Thereafter, the permeability undergoes different rebounds with continued injection as a result of reduced coal swelling effects (Masoudian et al., 2013) and the dominance of pore pressure effects. The pressure propagates fastest in Case B (green lines in Fig. 8b) and slowest in Case A (purple lines in Fig. 8b) that also affect the timing of thepermeability rebound. The results in Fig. 8 show that an increase of Poisson's ratio υ and a decrease of Young's modulus E can be beneficial in promoting rebound of permeability. Indeed, with the combination of varying E and υ , Case D displays the largest permeability (rebound) and pore pressure at later time (red lines in Fig. 8a and 8b).

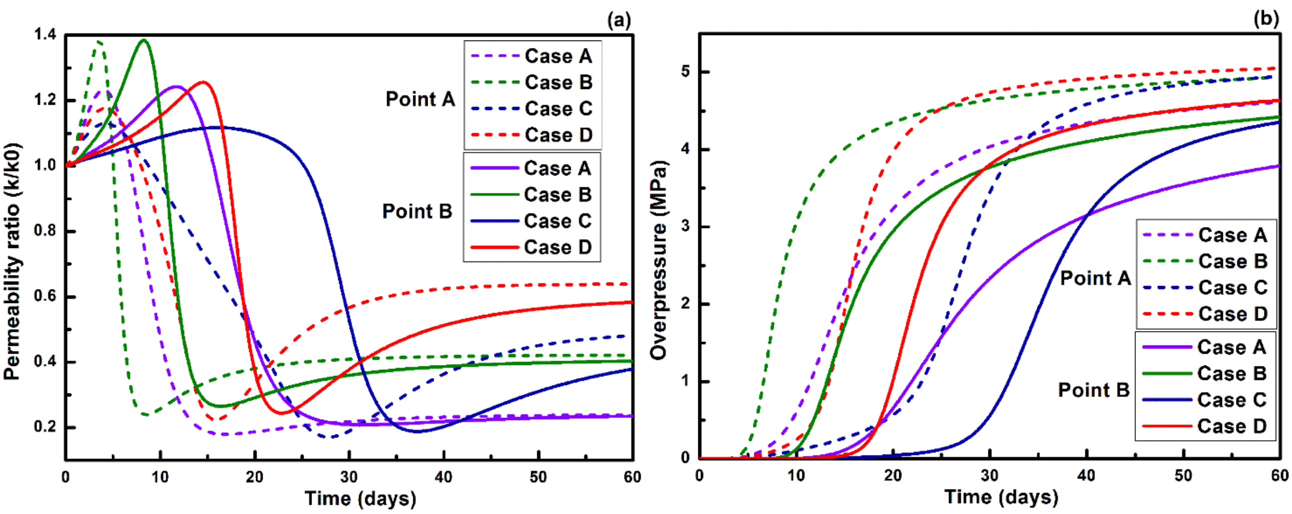

Fig. 8. (a) Permeability (b) pore pressure in the coal seam versus time at different points within the coal seam.

Fig. 9 shows a comparison of CO_2 injection rate and cumulative CO_2 injection for the four cases of constant or variable elastic properties The CO_2 injection rate Q_d is defined as

$$u\,dA = 2*¿\int u*1\,dl\,(18)$$
$$Q_d = 2*\int ¿$$

where u is the CO_2 fluid velocity through the injection boundary, which is directly extracted from simulation results in COMSOL. The cumulative injection Q_t is calculated by

$$Q_t = \int Q_d\,dt\,(19)$$

In Eq. (18), A is the injection area representing the horizontal well surface area, where l is the vertical thickness of the injection element ($l=0.1$) and the factor 1 correspond to 1 m of the horizontal well. Thus, the injection rate and cumulative injection in Fig. 9 are per meter well, whereas the total injection rate and cumulative injection volume would be obtained by multiplying with the total length of the horizontal injection rate.

In all four cases an initial peak in the CO_2 injection rate occurs in the first few hours of injectiona result of a large pressure contrast between injection pressure and initial pore pressure in the coal seam (Fig. 9a). At early time, the injection rate and cumulative injection in Case B (green lines in Fig. 9a and 9b) are larger than in other cases for its larger enhancement of permeability (green lines in Fig. 8a). With continued CO_2 injecting, the injection rate in Case D exceeds others (red line in Fig. 9a), which tends to decrease the difference of cumulative injection between Case B and D (green and red lines in Fig. 9b). Towards the end of the simulation Case D cumulative injection exceeds that of Case B for its continued high daily injection (red line in Fig. 9). The higher injection rate at later times in the case of a softening modulus and an increasing υ are attributed to the stronger permeability rebound in Case D (red lines in Fig. 8a) that accelerates gas pressure and CO_2 propagation into the coal seam. This demonstrates that the CO_2-induced softening of the elastic modulus and rising of Poisson's ratio can enhance CO_2 injectivity and storage capacity for a long-term CO_2 injection into deep coal seams.

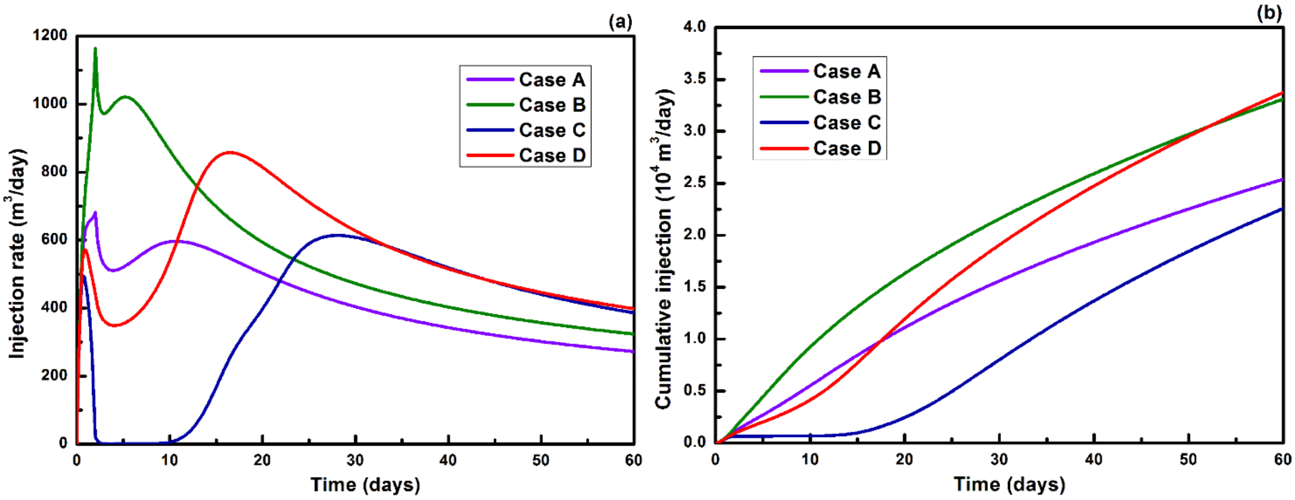

Fig. 9. (a) CO_2 injection rate and (b) cumulative CO_2 injection versus time for four different cases.

The injection-induced increase in pore pressure within the coal seam gives rise to vertical displacement in the caprock as shown in Fig. 10. At early stages, the vertical displacements in Case B (green solid lines in Fig. 10a) are larger than for the three other cases, but towards the end of the 60 days injection, the displacements magnitudes are the largest for Case D. The evolution and distribution of vertical displacements in Fig. 10 generally follow the pore pressure evolution in Fig. 8b and distribution in Fig. 6. This shows that the adsorption induced changed in elastic properties affects coal permeability and pressure diffusion that in turn affect the vertical expansion and uplift. The uplift can be observed far away (150 and 200 m) from the injection boundary, and the maximum uplift in the case of softening elastic modulus E and increasing Poisson's ratio υ is approximately 120 mm (red solid line in Fig. 10b), about 22 mm larger than that in the case of constant E and υ (purple solid line in Fig. 10b).

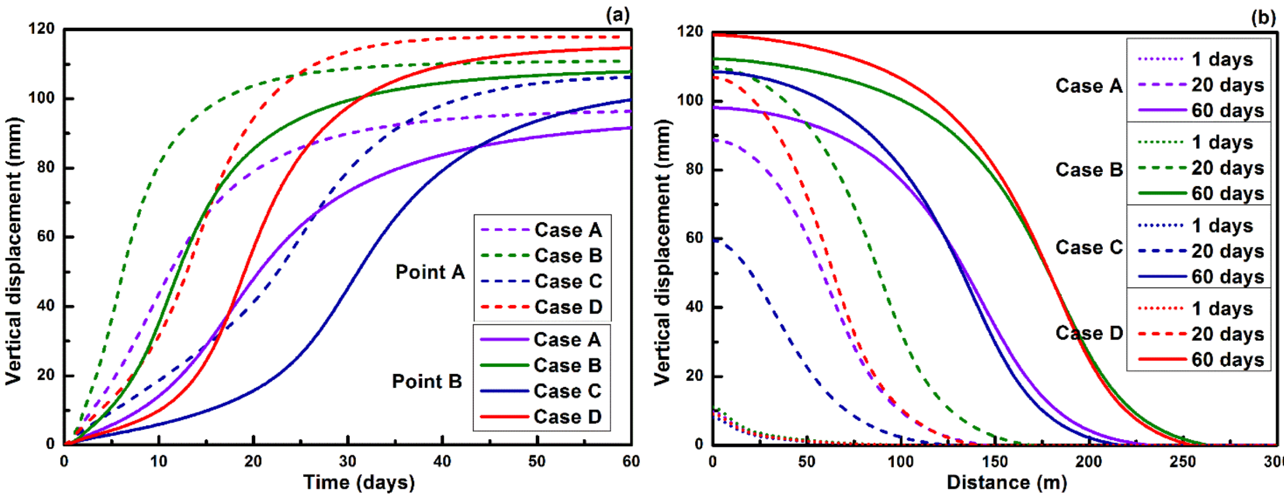

Fig. 10. (a) Vertical displacement versus time at points C and D in the caprock (b) Vertical displacement along cross-section B in the caprock 6.7 m above the coal seam after 1, 20 and 60 days of injection.

5.2 Sensitivity analysis

The following subsections (5.2.1-5.24) present a sensitivity analysis to study how the CO_2 injection performance depends on coefficients a and b related to CO_2-adsorption-induced changes in elastic properties, hydraulic properties (porosity and permeability) and initial elastic properties (Young's modulus and Poisson's ratio) of coal seams, as well as how the injection pressure affects the performance of the CO_2 injection. In particular, we study the injection rate, cumulative injection and the evolution of parameters at two control points in the model domain. We present the evolution of pore pressure, elastic modulus and permeability at point A, which is located at a distance of 30 m away from the injection wellbore and at the mid-elevation of the coal seam. We also present vertical displacement at point C, located in the caprock 6.7 m above the coal seam.

5.2.1 Effect of coefficients a and b

Fig. 11 shows the effect of coefficients a (0.1 and 0.3) and b (0.1 and 0.3) on hydromechanical parameters; the time-evolutions of overpressure, elastic modulus, permeability ratio, injection rate, cumulative injection and vertical displacement. The elastic properties of different coal seams may be more or less sensitivity to CO_2 adsorption, which in our model correspond to different values ofcoefficients a and b. The value of a and b are may be related to the *in-situ* stress state (uniaxial or triaxial compression), mechanical properties (elastic modulus and Poisson's ratio) and components (clay, sand or other mineralogy) of coal (Levine, 1996; Viete and Ranjith, 2006; Hol et al., 2011; Masoudian et al., 2014; Mishra and Dlamini, 2012; Masoudian et al., 2014). The equation for the softening of the elastic modulus as a function of overpressure implies that a larger value of a induces more elastic modulus softening. The Young's modulus is reduced to 21.3% of its initial value when $a=0.3$, but only to 68.9% when $a=0.1$ (dashed lines in Fig. 11a).

At early stages, the coal with a smaller a and same $b=0.1$ result in a larger overpressure, permeability, injection rate and deformation (purple vs blue line in Fig.11). At later stages, more CO_2 is injected into the coal seam for higher values of a (blue solid line in Fig. 11c) and the final cumulative injection at 60 days are close in the two cases with different a (purple vs blue dashed line in Fig. 11c). Among the three cases, the pressure propagates fastest for a coal with larger a and b that results in the highest injection rate, permeability peak and rebound, cumulative injection and deformation (red lines in Fig. 11). As noted previously in this paper, an increase of Poisson's ratio can promote the enhancement of permeability, whereas a decrease of Young's modulus has the opposite effect at the early stages. Compared this conclusion with permeability variations in Fig. 11b, it infers that coefficient a is more influential than coefficient b at early time. Later, under the combination of a smaller modulus and larger Poisson's ratio, the permeability can rebound earlier (red line in Fig. 11b).

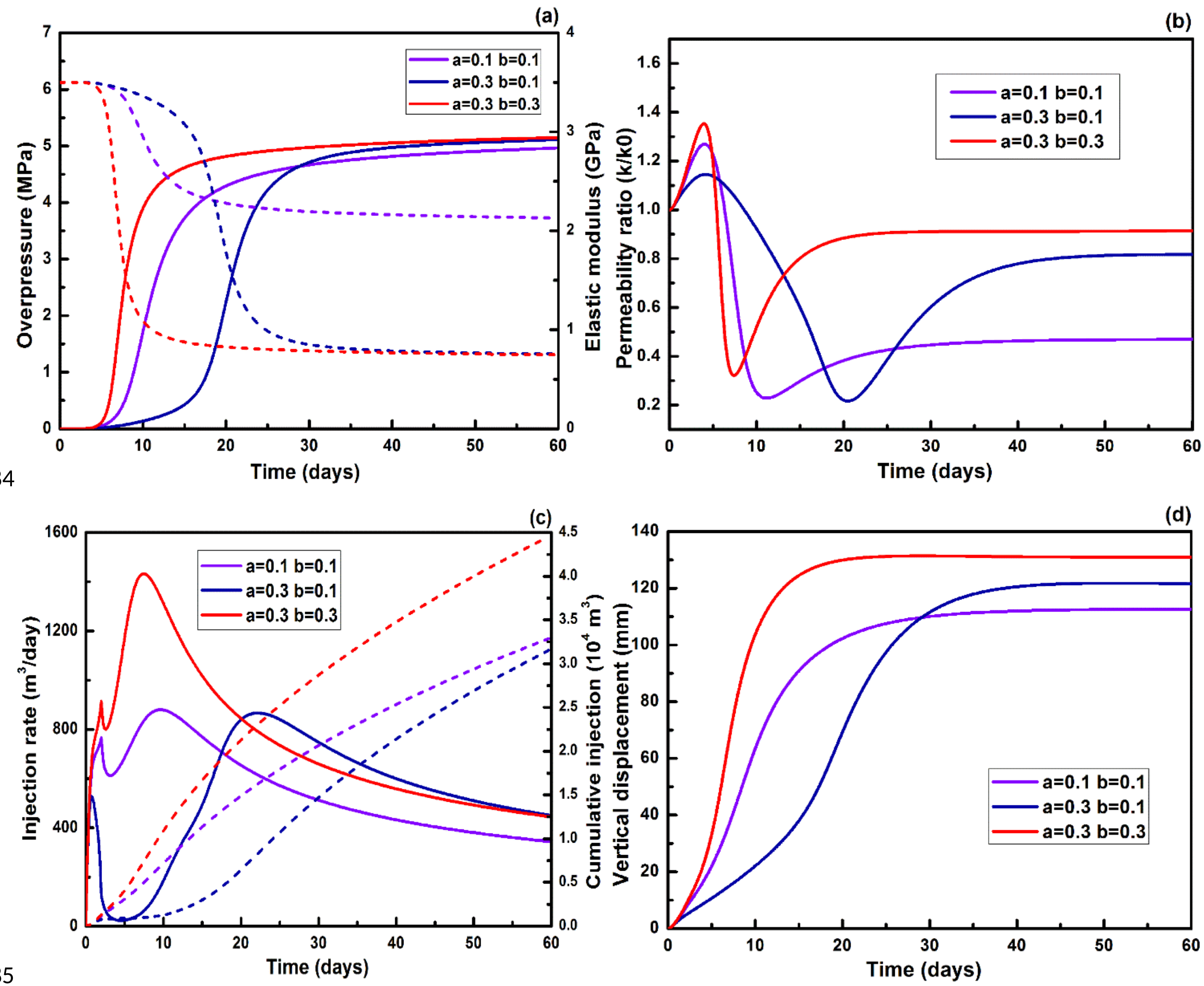

Fig. 11. Effect of coefficient a and b on (a) pore pressure and elastic modulus, (b) permeability, (c) injection rate and cumulative injection, and (d) vertical displacement. An initial reference porosity of 0.8%, permeability of 1×10^{-14} m^2, injection pressure of 6 MPa and an initial coal-seam pressure of 0.5 MPa are applied in all simulations.

5.2.2 Effect of hydraulic properties (permeability and porosity)

Permeability of the cleat system is recognized as one of the most important parameters for the injectivity into coal seams (Wei and Zhang, 2010). Varying permeability and related porosity result in large changes in overpressure, which then in turn affects elastic modulus, Poisson's ratio, permeability changes, injection rate, cumulative injection and vertical displacement (Fig. 12). In a coal-seam with a higher permeability and same porosity, the gas overpressure front and CO_2 reaches the same distance away from the wellbore in a shorter time. For example, in the case of a relatively high initial permeability $k_0 = 1 \times 10^{-14}$ m^2, the gas pressure front reaches point A after about 2 days of injection, while it takes approximately 4 days with a smaller permeability of $5 \times 10^{-15} m^2$

(red vs green solid line in Fig. 12a). In other words, in the case of higher permeability more CO_2 can be injected and adsorbed inside a coal seam over the same injection time period. The permeability deceases to 90% of its original value for the case with a high porosity ($\phi_0=8$) (red and green lines in Fig. 12b) and as low as 20% of initial permeability (blue and purple lines in Fig. 10b) for a case with a small porosity ($\phi_0=0.8$). This also contributes to improve CO_2 daily and cumulative injection efficiency (dashed and solid lines in Fig. 12c). In other words, the initial porosity is more influential than initial permeability on the change of permeability and CO_2 injection. Higher initial porosity and permeability are preferable for the improvement of CO_2 injection efficiency into coal seams. The higher overpressure and corresponding softening of elastic modulus also cause a larger deformation in the caprock (Fig. 12d).

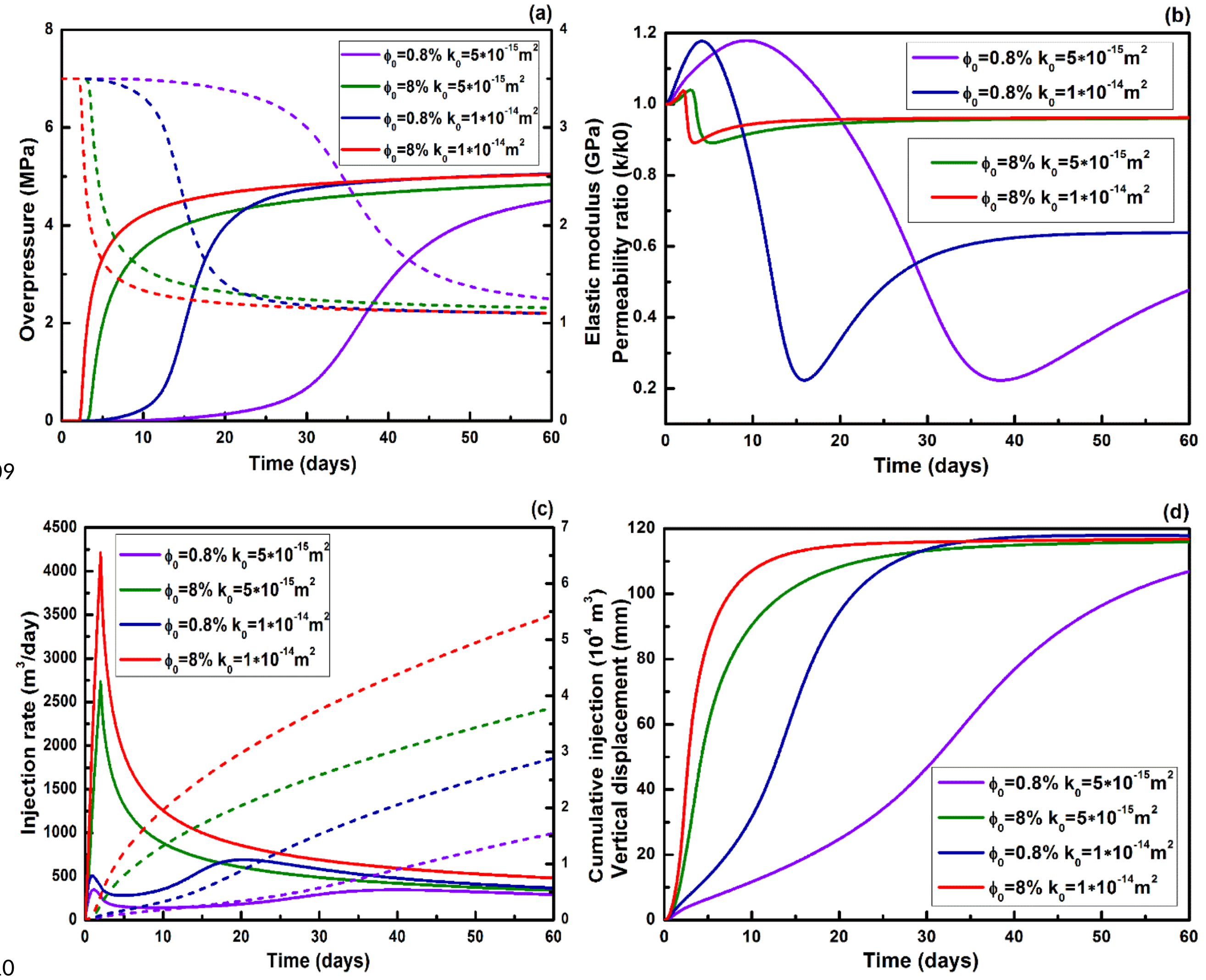

Fig. 12. Effect of hydraulic properties on (a) pore pressure and elastic modulus (b) permeability (c) injection rate and cumulative injection (d) vertical displacement. The coal seam has an initial reference cleat system porosity of 0.8% or 8% and an initial reference permeability of 1 × 10^{-14} or 5 × 10^{-15} m^2. A softening coefficient of 0.2291, an injection pressure of 6 MPa and initial coal-seam pressure of 0.5 MPa are applied in all simulations.

5.2.3 Effect of elastic properties (Young's modulus and Poisson's ratio)

The coal mechanical properties (Young's modulus E and Poisson's ratio υ) control the variation of permeability (Bustin and Bustin, 2012) that affects the CO_2 injection efficiency. Fig. 13 presents hydromechanical parameters versus time for various Young's modulus E and Poisson's ratio υ. For a coal with a larger Poisson's ratio ($\upsilon=0.35$) and same E, the injection efficiency of CO_2, permeability peak and caprock deformation are larger than a coal with a small υ (green vs purple and red vs blue lines in Fig.11). For a coal with a larger Young's modulus ($E=3.5\,GPa$), the pore pressure is obviously higher (red and blue solid lines in Fig.11a) that causes larger changes of modulus (red and blue dashed lines in Fig.11a) and Poisson's ratio with continued injecting. The permeability in the four cases displays similar trends with an increase during the first few days and then a decrease. The permeability undergoes a significant rebound from around 15 and 40 days of injection (red and blue lines in Fig.11b). At the later time, no recovery of permeability (green and purple lines in Fig.11b) occurs for the smaller pore pressure and the higher rebound pressure in a stiffer coal with larger Young's modulus (green and purple dashed lines in Fig.11a). Consequently, less CO_2 injection rate and caprock deformation are predicted for a coal with smaller E (blue and purple lines in Fig.13c and 13d). Overall, initial Passion's ratio is less influential than initial Young's modulus on permeability rebound. The larger pore pressure and more soft coal with a smaller E cause larger deformation in the caprock (Fig.13d).

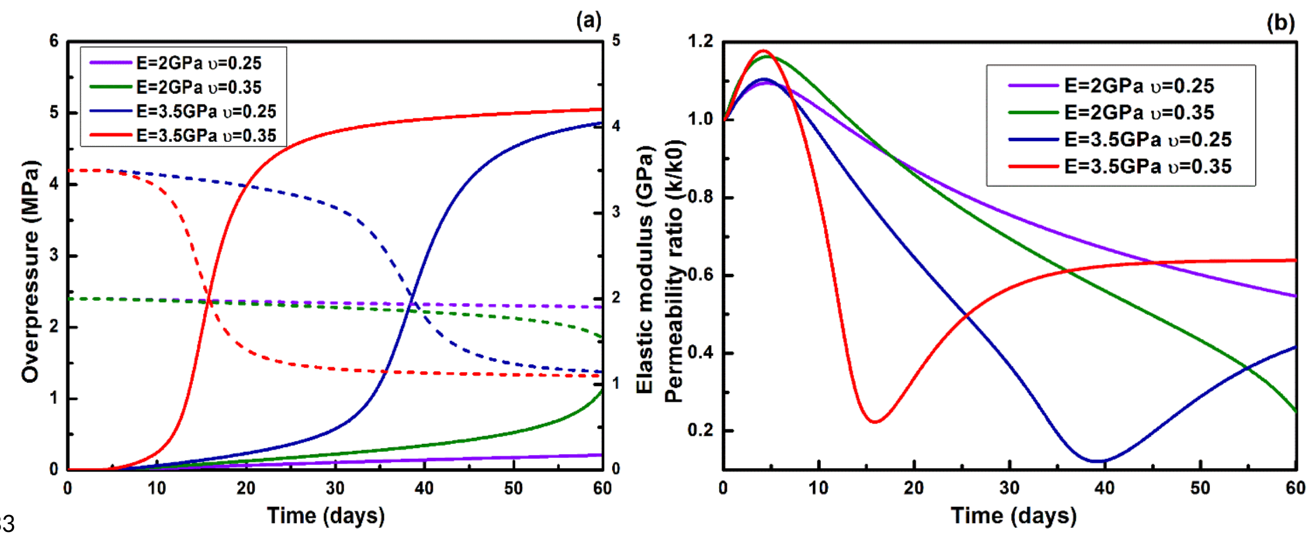

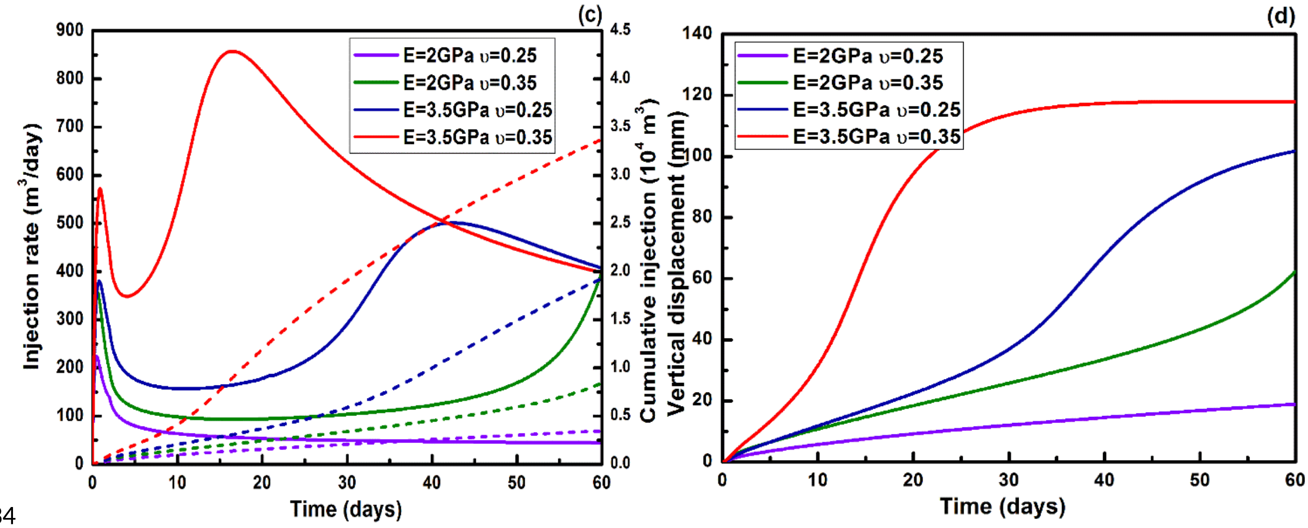

Fig. 13. Effect of initial Young's modulus and Poisson's ratio property on (a) pore pressure and elastic modulus, (b) permeability ratio, (c) injection rate and cumulative injection, and (d) vertical displacement. An initial reference porosity of 0.8%, an initial reference permeability of 1 × 10^{-14} m^2, softening coefficient of 0.2291 and an injection pressure of 6 MPa are applied in all simulations.

5.2.4 Effect of injection pressure

The evolution of overpressure, elastic modulus, permeability ratio and vertical displacement for different injection pressures is shown in Fig. 14. The injection pressure governs the total amount of CO_2 that can be injection into a coal seam (Cui and Bustin, 2005); CO_2 can be injected at a higher rate and more CO_2 can be adsorbed with a high injection pressure. For coal seams with same initial gas pressure, a higher injection pressure results in a higher coal-seam overpressure and injection rate peak (solid line in Fig. 14a and 14c). The higher overpressure, in turn, results in a greater elastic modulus softening (dashed lines in Fig. 12a) and Poisson's ratio rising, higher permeability increase, injectivity, and storage efficiency. Larger injection pressure advance the pore pressure to reach the rebound pressure that causes an earlier and larger rebound of permeability. The permeability undergoes a more significant rebound for the case with a higher injection pressure (Fig. 11b). The peak of injection rate and cumulative injection is correspondingly higher for the cases with a larger injection pressure (Fig. 11c).

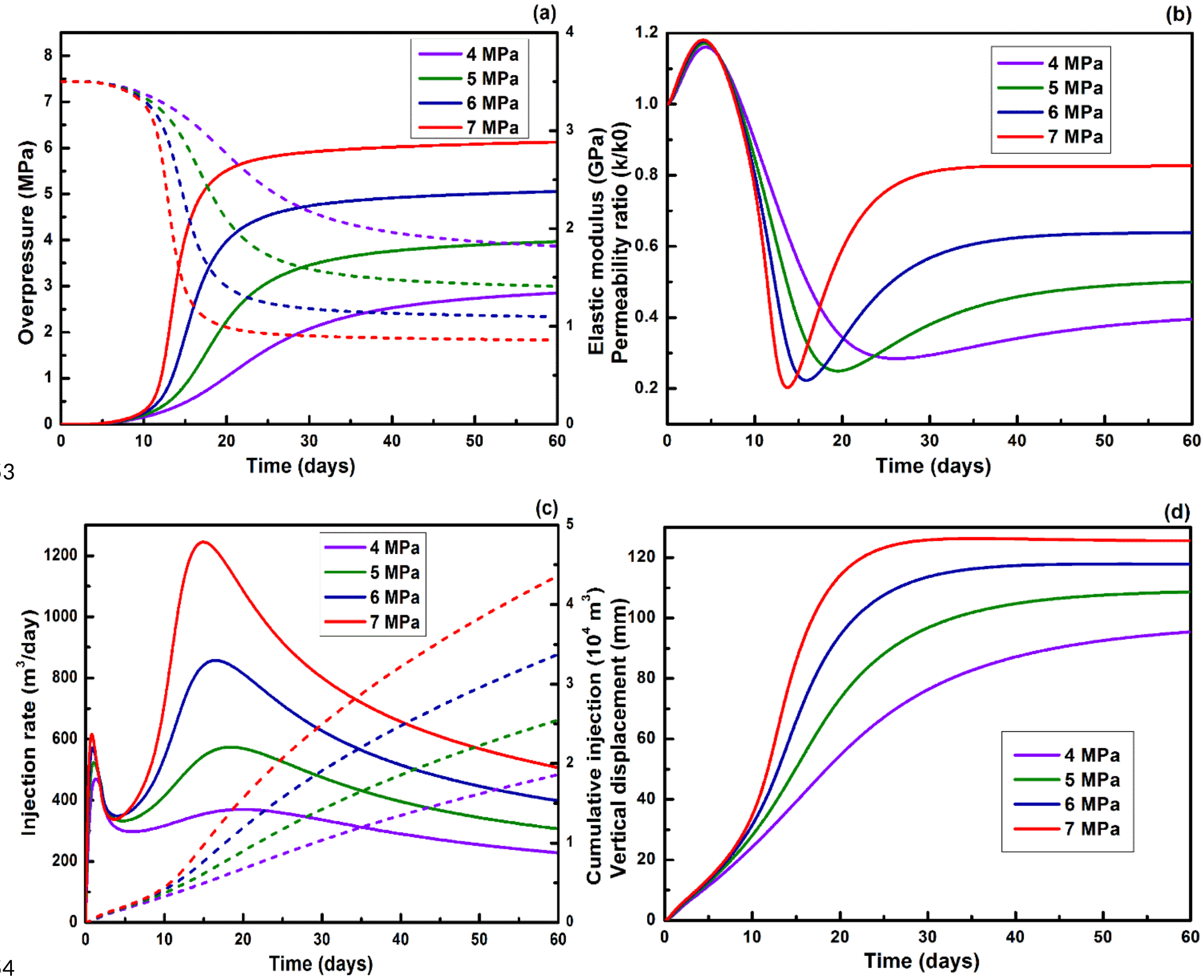

Fig. 14. Effect of injection pressure on (a) pore pressure and elastic modulus, (b) permeability, (c) injection rate and cumulative injection and (d) vertical displacement. An initial reference porosity of 0.8%, an initial reference permeability of 1 × 10^{-14} m^2, softening coefficient of 0.2291 and an initial coal-seam pressure of 0.5 MPa are applied in all simulations.

A high injection pressure helps improve the injectivity and storage efficiency, but it also leads to a larger rock deformation in the caprock. The vertical displacement (uplift) increases from approximately 95 to 125 mm when injection pressure increases from 4 to 7 MPa (Fig. 14d). Thus, it is necessary to consider potential impact of such uplift on the overburden integrity and surface structures when designing an injection operation for an efficient injection and acceptable uplift.

6. Conclusions

In this study, CO2 injection into coal seams was studied using a coupled flow-deformation model with a new stress-dependent porosity and permeability model that considers CO2-induced elastic property variation. This model incorporates free and adsorbed CO_2, coal deformation, and changes in elastic properties (Young's modulus and Poisson's ratio) with CO_2-content. Coefficients that govern changes in Young's modulus and Poisson's ratio with CO_2 pressure were determined from triaxial compression tests of coal samples extracted from the site of the first CO_2-ECBM recovery pilot tests in China. The triaxial compression tests shows that the elastic modulus softens and Poisson's ratio increases significantly with increasing CO_2 content when the CO_2-pressure increases from atmospheric to 4.52 MPa. The objective of this study is to investigate the effects of varying elastic properties on the performance of CO_2 sequestration into coal seams, including injectivity, stored mass (cumulative injection) and caprock deformation, and how such performance is affected by the evolution of parameters such as permeability, porosity, modulus and Poisson's ratio.

Simulation results showed that the injectivity, stored mass, and caprock deformation are significantly affected by the CO_2-induced changes in Young's modulus and Poisson's ratio.. At early stages of injection, an increase of Poisson's ratio promotes an increase of permeability that in increases the injection efficiency while the elastic modulus softening has anopposite effect of decreasing injection efficiency. With continued injecting, a decrease of elastic modulus has a dominated impact on reducing the rebound pressure required to rebound permeability, which significantly improves the longer term CO_2 injectivity and storage efficiency. However, a smaller elastic modulus and higher overpressure also lead to larger deformations in the caprock and overburden. A sensitivity study showed that hydromechanical characteristics including larger changes in elastic propertgies through coefficients a and b, high initial permeability and porosity, large initial Young's modulus and Poisson ratio and injection pressure all contribute synergistically to increase CO_2 injectivity and adsorption in coal seams, but also result in larger caprock deformations and uplift. Overall, the study shows the importance of considering the CO_2-induce elastic property variations when analyzing the performance and environmental impact of a CO_2-sequestration operation in uminable coal seams.

Appendix A

With consideration of the CO_2-sorption induced volumetric strain, the strain and stress relationship for a deforming coal seam is (Shi and Durucan, 2004)

$$\sigma'_{ij} = 2G\varepsilon_{ij} + \lambda\varepsilon_t\delta_{ij} - \left(\lambda + \frac{2}{3}G\right)\varepsilon_s\delta_{ij} \quad (A.1)$$

where ε_t is the bulk volumetric strain, δ_{ij} is the Kronecker symbol; ε_s is sorption-induced volumetric strain, G and λ are the Lame constants, described in terms of Young's modulus, E and Poisson's ratio, ν as

$$G=\frac{E}{2(1+\upsilon)},\lambda=\frac{E\upsilon}{(1+\upsilon)(1-2\nu)}$$

In this paper, the adopted sign convention is that tensile strain and stress are positive and compressive are negative. The effective stress σ' is calculated as

$$\sigma'_{ij}=\sigma_{ij}+\alpha p \delta_{ij} \quad (A.2)$$

where σ is the total stress. The Biot coefficient α is defined as

$$\alpha=1-\frac{K}{K_S}=1-\frac{E}{E_s} \quad (A.3)$$

where K and E is the bulk modulus and K_S is the modulus of the coal grains.

The bulk volumetric strain can be derived from Eq. (A.1) as

$$\varepsilon_t=\frac{dV_t}{V_t}=\frac{1}{K}(d\sigma+\alpha\, dp)+d\varepsilon_s \quad (A.4)$$

The pore volumetric strain can also be expressed as

$$\varepsilon_p=\frac{dV_p}{V_p}=\frac{1}{K_p}d\sigma+\left(\frac{1}{K_p}-\frac{1}{K_s}\right)dp+d\varepsilon_s \quad (A.5)$$

where V_t and V_p are the bulk and pore volumes, respectively; K_p is the pore modulus.

The fracture-cleat porosity of a coal seam is defined as

$$\phi=\frac{V_p}{V_t} \quad (A.6)$$

Thus, the porosity change of a deforming coal seam can be described as

$$d\phi=d\left(\frac{V_p}{V_t}\right)=\frac{V_p}{V_t}\left(\frac{dV_p}{V_p}-\frac{dV_t}{V_t}\right) \quad (A.7)$$

According to the Betti-Maxwell reciprocal theorem (Detournay and Cheng, 1993), K_p is a function of ϕ, described as

$$\frac{1}{K_p}=\frac{\alpha}{\phi}\frac{1}{K} \quad (A.8)$$

Substituting Eq. (A.8) into Eq. (A.7), then

$$\frac{d\phi}{\phi}=\left(\frac{\alpha}{\phi}\frac{1}{K}-\frac{1}{K}\right)(d\sigma+dp) \quad (A.9)$$

Integrating the equation yields

$$\phi=\alpha+(\phi_0-\alpha)\exp\left\{\frac{-1}{K}\left[(\sigma-\sigma_0)+(p-p_0)\right]\right\}(A.10)$$

Rewriting the Eq. (A.10) as a function of mean effective stress and pore pressure, it's expressed as

$$\phi=\alpha+(\phi_0-\alpha)\exp\left\{\frac{-1}{K}\left[(\sigma'-\sigma'_0)+(1-\alpha)(p-p_0)\right]\right\}(A.11)$$

By assuming $\alpha=1$, $K_p\ll K$ and K_p is a constant and simply approximated to be $K_p=\phi_0 K$, Eq. (A.9) can be integrated yielding

$$\phi=\phi_0\exp\left\{\frac{-1}{K_p}\left[(\sigma-\sigma_0)+(p-p_0)\right]\right\}(A.12)$$

By assuming $\phi\ll 1$, Eq. (A.9) can be integrated yielding

$$\phi=\phi_0+\frac{\alpha}{K}\left[(\sigma-\sigma_0)+(p-p_0)\right](A.13)$$

Without consideration of the Klinkenberg effect, a cubic law is used to describe the relationship between the permeability and porosity of the porous media, which is shown as follows

$$\frac{k}{k_0}=\left(\frac{\phi}{\phi_0}\right)^3=\left\{\frac{\alpha}{\phi_0}+\frac{(\phi_0-\alpha)}{\phi_0}\exp\left\{\frac{-1}{K}\left[(\sigma-\sigma_0)+(p-p_0)\right]\right\}\right\}^3(A.14)$$

$$\frac{k}{k_0}=\left(\frac{\phi}{\phi_0}\right)^3=\left\{\exp\left\{\frac{-1}{K_p}\left[(\sigma-\sigma_0)+(p-p_0)\right]\right\}\right\}^3(A.15)$$

$$\frac{k}{k_0}=\left(\frac{\phi}{\phi_0}\right)^3=\left\{1+\frac{\alpha}{K\phi_0}\left[(\sigma-\sigma_0)+(p-p_0)\right]\right\}^3(A.16)$$

Eqs. (A.15) and (A.16) are the C&B and P&M models (Cui and Bustin, 2005; Palmer and Mansoori, 1998), respectively, assuming that the reservoirs are under conditions of uniaxial strain, constant reservoir loading and $\alpha=1$. The horizontal stress σ_x or σ_y is given from equation (A.1) as

$$\sigma_x=\sigma_y=\frac{v}{1-v}\sigma_z-\frac{1-2v}{1-v}p-\frac{1-2v}{1-v}K\varepsilon_S(A.17)$$

Substituting Eq. (A.17) into Eq. (A.14), (A. 15) and (A.16) gives

$$\frac{k}{k_0}=\left\{\frac{\alpha}{\phi_0}+\frac{(\phi_0-\alpha)}{\phi_0}\exp\left\{\frac{-1}{K}\left[\frac{(1+v)}{3(1-v)}(p-p_0)-\frac{2E}{9(1-v)}(\varepsilon_s-\varepsilon_{s0})\right]\right\}\right\}^3(A.18)$$

$$\frac{k_{C\wedge B}}{k_0}=\exp\left\{\frac{3}{K_p}\left[\frac{(1+v)}{3(1-v)}(p-p_0)-\frac{2E}{9(1-v)}(\varepsilon_s-\varepsilon_{s0})\right]\right\}^3 \quad (A.19)$$

$$\frac{k_{P\wedge M}}{k_0}=\left\{1+\frac{1}{K_p}\left[\frac{(1+v)}{3(1-v)}(p-p_0)-\frac{2E}{9(1-v)}(\varepsilon_s-\varepsilon_{s0})\right]\right\}^3 \quad (A.20)$$

Acknowledgments

This study was supported by Special Subject Grant of National “973” Basic Research Program of China (No. 2015CB251602 and No.2009CB219605), National Natural Science Foundation of China (No. 41074040 and No. 50774083), Jiangsu Natural Science Foundation (No. BK20141125) and Chinese Program for New Century Excellent Talents in University (No. NCET-07-0803). The work was funded in part by the U.S. Department of Energy under contract no. DE-AC02-05CH11231. Special thanks to the anonymous reviewers for their valuable comments.

References

Ates, Y., Barron, K., 1988. The effect of gas sorption on the strength of coal. Mining Science and Technology 6, 291-300.

Bachu, S., 2008. CO2 storage in geological media: Role, means, status and barriers to deployment. Progress in Energy and Combustion Science 34, 254-273.

Bustin, A.M.M., Bustin, R.M., 2012. Importance of rock properties on the producibility of gas shales. International Journal of Coal Geology 103, 132-147.

Cui, X., Bustin, R.M., 2005. Volumetric strain associated with methane desorption and its impact on coalbed gas production from deep coal seams. AAPG Bulletin 89, 1181-1202.

Detournay, E., Cheng, A.H.-D., 1993. Fundamentals of Poroelasticity1.

Durucan, S., Shi, J.-Q., 2009. Improving the CO2 well injectivity and enhanced coalbed methane production performance in coal seams. International Journal of Coal Geology 77, 214-221.

Ferronato, M., Gambolati, G., Janna, C., Teatini, P., 2010. Geomechanical issues of anthropogenic CO2 sequestration in exploited gas fields. Energy Conversion and Management 51, 1918-1928.

Gale, J., 2004. Geological storage of CO2: What do we know, where are the gaps and what more needs to be done? Energy 29, 1329-1338.

Goodman, A.L., Favors, R.N., Larsen, J.W., 2006. Argonne coal structure rearrangement caused by sorption of CO2. Energy & Fuels 20, 2537-2543.

Gou, Y., Hou, Z., Liu, H., Zhou, L., Were, P., 2014. Numerical simulation of carbon dioxide injection for enhanced gas recovery (CO2-EGR) in Altmark natural gas field. Acta Geotech. 9, 49-58.

Gray, I., 1987. Reservoir engineering in coal seams: Part 1-The physical process of gas storage and movement in coal seams. SPE Reservoir Engineering 2, 28-34.

Haszeldine, R.S., 2009. Carbon Capture and Storage: How Green Can Black Be? Science 325, 1647-1652.

Hol, S., Peach, C.J., Spiers, C.J., 2011. Applied stress reduces the CO2 sorption capacity of coal. International Journal of Coal Geology 85, 128-142.

Kumar, H., Elsworth, D., Mathews, J.P., Liu, J., Pone, D., 2014. Effect of CO2 injection on heterogeneously permeable coalbed reservoirs. Fuel 135, 509-521.

Levine, J.R., 1996. Model study of the influence of matrix shrinkage on absolute permeability of coal bed reservoirs. Geological Society, London, Special Publications 109, 197-212.

Li, X., Fang, Z.-m., 2014. Current status and technical challenges of CO2 storage in coal seams and enhanced coalbed methane recovery: an overview. Int J Coal Sci Technol 1, 93-102.

Liu, H.-H., Rutqvist, J., 2010. A new coal-permeability model: internal swelling stress and fracture–matrix interaction. Transport in Porous Media 82, 157-171.

Masoudian, M., Airey, D., El-Zein, A., 2013. A chemo-poro-mechanical model for sequestration of carbon dioxide in coalbeds. Geotechnique 63, 235-243.

Masoudian, M.S., Airey, D.W., El-Zein, A., 2014. Experimental investigations on the effect of CO2 on mechanics of coal. International Journal of Coal Geology 128–129, 12-23.

Mishra, B., Dlamini, B., 2012. Investigation of Swelling and Elastic Property Changes Resulting from CO2 Injection into Cuboid Coal Specimens. Energy & Fuels 26, 3951-3957.

Palmer, I., Mansoori, J., 1998. How Permeability Depends on Stress and Pore Pressure in Coalbeds: A New Model.

Reucroft, P.J., Patel, H., 1986. Gas-Induced Swelling in Coal. Fuel 65, 816-820.

Rubin, E.S., 2005. IPCC Special Report on Carbon Dioxide Capture and Storage.

Rutqvist, J., Börgesson, L., Chijimatsu, M., Kobayashi, A., Jing, L., Nguyen, T.S., Noorishad, J., Tsang, C.F., 2001. Thermohydromechanics of partially saturated geological media: governing equations and formulation of four finite element models. International Journal of Rock Mechanics and Mining Sciences 38, 105-127.

Rutqvist, J., Tsang, C.F., 2002. A study of caprock hydromechanical changes associated with CO2-injection into a brine formation. Environmental Geology 42, 296-305.

Seidle, J.P., Huitt, L., 1995. Experimental measurement of coal matrix shrinkage due to gas desorption and implications for cleat permeability increases, International meeting on petroleum Engineering, pp. 575-582.

Shi, J.Q., Durucan, S., 2004. Drawdown Induced Changes in Permeability of Coalbeds: A New Interpretation of the Reservoir Response to Primary Recovery. Transport in Porous Media 56, 1-16.

Shukla, R., Ranjith, P., Haque, A., Choi, X., 2010. A review of studies on CO2 sequestration and caprock integrity. Fuel 89, 2651-2664.

Siriwardane, H., Haljasmaa, I., McLendon, R., Irdi, G., Soong, Y., Bromhal, G., 2009. Influence of carbon dioxide on coal permeability determined by pressure transient methods. International Journal of Coal Geology 77, 109-118.

Van Bergen, F., Gale, J., Damen, K., Wildenborg, A., 2004. Worldwide selection of early opportunities for CO2-enhanced oil recovery and CO2-enhanced coal bed methane production. Energy 29, 1611-1621.

Viete, D.R., Ranjith, P.G., 2006. The effect of CO2 on the geomechanical and permeability behaviour of brown coal: Implications for coal seam CO2 sequestration. International Journal of Coal Geology 66, 204-216.

Warren, J.E., Root, P.J., 1963. The Behavior of Naturally Fractured Reservoirs. Society of Petroleum Engineers Journal 3, 245-255.

Wei, Z., Zhang, D., 2010. Coupled fluid-flow and geomechanics for triple-porosity/dual-permeability modeling of coalbed methane recovery. International Journal of Rock Mechanics and Mining Sciences 47, 1242-1253.

White, C.M., Smith, D.H., Jones, K.L., Goodman, A.L., Jikich, S.A., LaCount, R.B., DuBose, S.B., Ozdemir, E., Morsi, B.I., Schroeder, K.T., 2005. Sequestration of carbon dioxide in coal with enhanced coalbed methane recovery a review. Energy & Fuels 19, 659-724.

Wong, S., Law, D., Deng, X., Robinson, J., Kadatz, B., Gunter, W.D., Jianping, Y., Sanli, F., Zhiqiang, F., 2007. Enhanced coalbed methane and CO2 storage in anthracitic coals—Micro-pilot test at South Qinshui, Shanxi, China. International Journal of Greenhouse Gas Control 1, 215-222.

Wong, S., Macdonald, D., Andrei, S., Gunter, W.D., Deng, X., Law, D., Ye, J., Feng, S., Fan, Z., Ho, P., 2010. Conceptual economics of full scale enhanced coalbed methane production and CO2 storage in anthracitic coals at South Qinshui basin, Shanxi, China. International Journal of Coal Geology 82, 280-286.

Zakkour, P., Haines, M., 2007. Permitting issues for CO2 capture, transport and geological storage: A review of europe,

USA, Canada and Australia. International Journal of Greenhouse Gas Control 1, 94-100.
Zhang, H., Liu, J., Elsworth, D., 2008. How sorption-induced matrix deformation affects gas flow in coal seams: A new FE model. International Journal of Rock Mechanics and Mining Sciences 45, 1226-1236.